water

MDPI

Article

Hydrological Dynamics and Climate Variability in the Sava River Basin: Streamflow Reconstructions Using Tree-Ring-Based Paleo Proxies

Abel Andrés Ramírez Molina [1], Igor Leščešen [2], Glenn Tootle [3,*], Jiaqi Gong [1] and Milan Josić [4]

[1] Department of Computer Science, The University of Alabama, Tuscaloosa, AL 35487, USA; aaramirez@crimson.ua.edu (A.A.R.M.); jiaqi.gong@ua.edu (J.G.)
[2] Institute of Hydrology, Slovak Academy of Sciences, Dúbravská cesta 9, 841 04 Bratislava, Slovakia; lescesen@uh.savba.sk
[3] Department of Civil, Construction and Environmental Engineering, The University of Alabama, Tuscaloosa, AL 35487, USA
[4] Department of Geography, Tourism and Hotel Management, Faculty of Sciences, University of Novi Sad, Trg Dositeja Obradovića 3, 21000 Novi Sad, Serbia; milan.josic@dgt.uns.ac.rs
* Correspondence: gatootle@eng.ua.edu; Tel.: +1-307-399-6666

Abstract: This study reconstructs historical streamflow in the Sava River Basin (SRB), focusing on hydrological variability over extended timescales. Using a combination of Machine Learning (ML) and Deep Learning (DL) models, streamflow patterns were reconstructed from self-calibrated Palmer Drought Severity Index (scPDSI) proxies. The analysis included nine ML models and two DL architectures, with a post-prediction bias correction applied uniformly using the RQUANT method. Results indicate that ensemble methods, such as Random Forest and Gradient Boosted Tree, along with a six-layer DL model, effectively captured streamflow dynamics. Bias correction improved predictive consistency, particularly for models exhibiting greater initial variability, aligning predictions more closely with observed data. The findings reveal that the 2000–2022 period ranks as the lowest 23-year flow interval in the observed record and one of the driest over the past ~500 years, offering historical context for prolonged low-flow events in the region. This study demonstrates the value of integrating advanced computational methods with bias correction techniques to extend hydrological records and enhance the reliability of reconstructions. By addressing data limitations, this approach provides a foundation for supporting evidence-based water resource management in Southeastern Europe under changing climatic conditions.

Keywords: streamflow reconstruction; Sava River Basin; ensemble methods; machine learning; deep learning; hydrological prediction

Academic Editor: Alexander Shiklomanov

Received: 25 December 2024
Revised: 29 January 2025
Accepted: 31 January 2025
Published: 2 February 2025

Citation: Ramírez Molina, A.A.; Leščešen, I.; Tootle, G.; Gong, J.; Josić, M. Hydrological Dynamics and Climate Variability in the Sava River Basin: Streamflow Reconstructions Using Tree-Ring-Based Paleo Proxies. *Water* **2025**, *17*, 417. https://doi.org/10.3390/w17030417

1. Introduction

Rivers serve as essential lifelines, providing vital water resources to communities globally. Over recent decades, population growth, climatic changes, and groundwater overuse have increased pressures on these critical water sources [1,2]. Unfortunately, many regions grapple with insufficient monitoring infrastructure, temporal and spatial data gaps, and data quality issues, complicating effective water resource management. This challenge is particularly pronounced in Southeastern Europe, where observational records usually span less than a century, failing to capture the long-term hydrological variability necessary for comprehensive understanding and management [3]. To address this limitation, innovative approaches such as the reconstruction of historical streamflow using

paleo-indicators have emerged as promising tools to extend hydrological records beyond the instrumental period [4,5]. Dendrohydrology, the science of using tree-ring data to reconstruct past hydrological variations, has gained prominence for its ability to provide detailed and continuous streamflow records [6–8].

Past research has evaluated the paleoclimate records of temperature and hydroclimate variability in the region [9–12]. While streamflow reconstructions are generally limited on the European continent, recent studies have successfully reconstructed streamflows of both the Danube River (DR) and the Sava River (SR). A notable ~250-year streamflow re-construction of the DR near Tulcea, Romania, utilized a tree-ring chronology dating from 1728 to 2020 from oak trees (*Quercus* sp.). The highest correlation value between DR streamflow and the tree-ring chronology was found for the November (previous year) to July (current year) streamflow season [13]. Similarly, a ~500-year streamflow reconstruction near Orsova, Romania, incorporated data from the Old World Drought Atlas (OWDA), which includes the self-calibrated Palmer Drought Severity Index (scPDSI) derived from summer-related tree-ring proxies [14]. Perhaps the most important contribution in the region is reconstructions of the seasonal streamflow in the Sava River in Slovenia, where the Stepwise Linear Regression (SLR) method was successfully applied to tree-ring-based scPDSI proxies. This study revealed both low-flow (drought) and high-flow (pluvial) periods over various time filters [11]. Previously, the reconstruction of SR summer streamflow in Croatia was conducted where a tree-ring chronology for narrow-leaved ash trees was developed and correlated with streamflow data from a gauge near Jasenovac station. Significant correlations were found between May, July, and August streamflows and the tree-ring chronology, as well as for the May–June–July–August streamflow season [15]. Notably, positive and significant correlations were observed between scPDSI and streamflow from March to October, with July and August scPDSI correlations exceeding those of the tree-ring chronology [11,15]. While these correlations primarily involve streamflow [11,15], the relationship between scPDSI and precipitation in the Sava River Basin (SRB) has also been explored [12], further supporting the use of scPDSI as a robust proxy for hydrological reconstructions in the SRB.

Additionally, recent advances in Machine Learning (ML) and Deep Learning (DL) have shown significant potential in hydrological reconstruction. The study in [12], focusing on SRB in Slovenia, demonstrated that ML and DL methods outperformed traditional regression techniques, including SLR, in reconstructing precipitation using scPDSI as a proxy. This highlights the capability of advanced algorithms to capture complex relationships between proxies and hydrological variables, offering a complementary approach to traditional methods.

Recent evidence indicates significant hydroclimatic changes in Southeastern Europe, including a consistent decrease in annual streamflow from mountain headwaters [16], an increase in March–July temperatures, reductions in the snow-to-rain ratios, more extreme precipitation events, and higher flood frequencies [17]. These changes align with the projected impacts of warming temperatures on precipitation variability [18], particularly in areas like the SRB. However, due to the lack of long-term hydrologic records, it is unclear whether these changes represent a shift to new conditions associated with warmer temperatures or a return to previous conditions not captured in the short observational record.

The Sremska Mitrovica gauge near the Croatian–Serbian border has kept a continuous record of daily discharge from 1926 to 2022. This strategically located gauge is crucial for monitoring the discharge dynamics of the water transfer from Croatia to Serbia. Given its importance, particularly under the Sava River Commission's responsibility for flood risk and sediment load management, extending the records of this gauge holds significant value. We have used these extensive records of river flow to reconstruct discharge patterns

using proxies derived from tree rings, whose records are much older than the instrumental data. Previous successful hydrological reconstructions in the United States [19], northern Italy [20,21], and Slovenia [11,12] have used the tree-ring-derived scPDSI as a proxy. Building on the significant positive correlation between scPDSI and SR discharge [11,15], and inspired by the demonstrated success of ML and DL in reconstructing hydrological variables [12], we used scPDSI as a proxy for the reconstruction to assess seasonal discharge reconstruction potential in the SRB. This research presents the first-known streamflow reconstruction of the SR in Serbia.

Although considerable progress has been made in the reconstruction of river courses, there are still significant gaps in research, particularly in Southeastern Europe, where few comprehensive historical river course reconstructions exist. Recent efforts have led to promising results, including reconstructions for the DR and the SR [11,13,15]. However, there is still a notable spatial gap in historical flow reconstructions for rivers in Southeastern Europe. Therefore, this study aims to achieve the following:

- Reconstruct the historical discharge of rivers in Southeastern Europe, specifically the Sava River.
- In lieu of traditional regression approaches, incorporate advanced ML and DL techniques using proxies derived from tree rings and discuss the advantages and disadvantages of the various approaches.
- Apply established bias correction methods to refine predictive accuracy.
- Upon developing skillful ML and DL reconstructions of discharge, provide a paleo perspective of the recent (2000 to 2022) 23-year drought.

The contribution of the current research was a deeper understanding of long-term hydrological variability and a transformative framework (ML/DL tree-ring-based proxy streamflow reconstructions) for improving water resource management strategies in Southeastern Europe.

2. Study Area

The Sava River Basin (SRB) (Figure 1), covering approximately 97,000 km², is the largest river basin in southeastern Europe and the second largest within the Danube basin. This basin spans several countries, including Serbia, Croatia, Slovenia, Bosnia and Herzegovina, and a small portion of Albania [22]. Originating in Slovenia, the Sava River (SR) forms from the confluence of the Sava Dolinka and Sava Bohinjka rivers near Radovljica. The river passes through diverse landscapes and climatic zones, receiving water from key tributaries like the Kolpa, Una, Vrbas, Bosna, Drina, and Kolubara. Notably, the southern tributaries, particularly in Bosnia, significantly influence the river's flow dynamics. Stretching 945 km from its source to its confluence with the Danube in Belgrade, Serbia, the SR sustains around 8 million inhabitants in its basin [18]. This population depends on the river for various socioeconomic activities, highlighting its critical role in regional development and livelihoods. The Sremska Mitrovica station in Serbia is located 139.2 km upstream of the Danube River (DR), covering an area of 87,996 km², which constitutes about 90.71% of the entire basin. This station is crucial for observing and evaluating hydrological processes within the Sava River catchment area. The basin features distinct climatic gradients, transitioning from a mountainous climate in the upper reaches to a temperate continental climate along the river's course. The Dinaric Mountains and the Pannonian Plain create climatic variations across the basin, resulting in alpine, temperate continental, and Peripannonian climates [22,23]. Precipitation varies significantly within the basin. Slovenia sees average annual precipitation of between 1570 mm and 2210 mm, with marked seasonal changes. In Croatia, the average is about 855 mm, reflecting diverse climatic influences [24,25]. Serbian regions, including around the Sremska Mitrovica station,

experience an average of 577 mm annually, with the highest rainfall in June and the lowest in February [25].

Figure 1. Sava River Basin showing the location of the Sremska Mitrovica gauging station.

The hydrological systems in the Sava basin exhibit varied characteristics, shifting from alpine nival–pluvial systems upstream to Peripannonian and Pannonian pluvial–nival systems downstream. The seasonal runoff dynamics at the Sremska Mitrovica gauging station reflect the complex interplay of climatic, topographical, and hydrological factors influencing the Sava River Basin [26]. The highest discharge values are observed in spring (March–May), primarily driven by snowmelt contributions from upstream alpine regions. Winter (December–February) runoff remains elevated due to precipitation, mainly as rain, and occasional snowmelt events in the middle and lower parts of the basin. This combination leads to runoff peaks in late winter and early spring, characteristic of mixed pluvial–nival hydrological regimes. In contrast, summer (June–August) and fall (September–November) exhibit significantly lower discharge values, with summer being the driest period due to high evapotranspiration rates and reduced precipitation typical for the warm continental climate of the Lower Sava Basin. In the fall, discharge values recover slightly due to increased precipitation, although the effects of the summer drought often persist [27]. Significant inter-annual fluctuations in discharge include notable peaks in spring and winter, such as during the extreme flood event of 2014 caused by intense rainfall. At the Sremska Mitrovica station, pronounced low water levels frequently occur during summer and early fall, exacerbated by the flat topography of the Pannonian Basin, high temperatures, and anthropogenic factors such as water extraction and upstream reservoir operations [28].

3. Materials and Methods

3.1. Observed Streamflow and Proxy Data

In this study, we utilized a 97-year dataset of daily discharges of the Sava River at the Sremska Mitrovica station in Serbia. The dataset, spanning from 1926 to 2022, was

obtained from the national water authority, Republic Hydrometeorological Service of Serbia (RHSS). Data quality control measures were rigorously implemented by RHSS, adhering to strict standards to ensure the accuracy and consistency of the data series used in this study. These measures included following their internal instructions as well as the recommendations of the World Meteorological Organization (WMO). This comprehensive approach ensured that the data were reliable and suitable for detailed hydrological analysis and reconstruction efforts. The daily discharges were aggregated to monthly, and the April–May–June–July–August–September (AMJJAS) season was selected, as this period represents the hydrological summer. In reviewing the observed dataset, 2022 represented the end-year of the lowest streamflow in the observed record for multiple drought periods including the following: 3 years (2020–2022), 4 years (2019–2022), 16 years (2007–2022), 17 years (2006–2022), 20 years (2003–2022), 21 years (2002–2022), 23 years (2000–2022), 24 years (1999–2022), and 25 years (1998–2022). The 23-year (2000–2022) period was selected for this study based on this period covering the 21st century.

To reconstruct streamflow, we employed self-calibrated Palmer Drought Severity Index (scPDSI) data derived from the Old World Drought Atlas (OWDA). The OWDA provides annual scPDSI values from 0 to 2012 AD across 5414 grid points in Europe [14]. For this study, we selected 247 scPDSI cells located within a 450 km radius of the Sremska Mitrovica gauge (44.96704° N, 19.60210° E) per [19]. The spatial distribution of these cells is shown in Figure 2, where the green dot represents the gauge location and red dots indicate the selected scPDSI grid points.

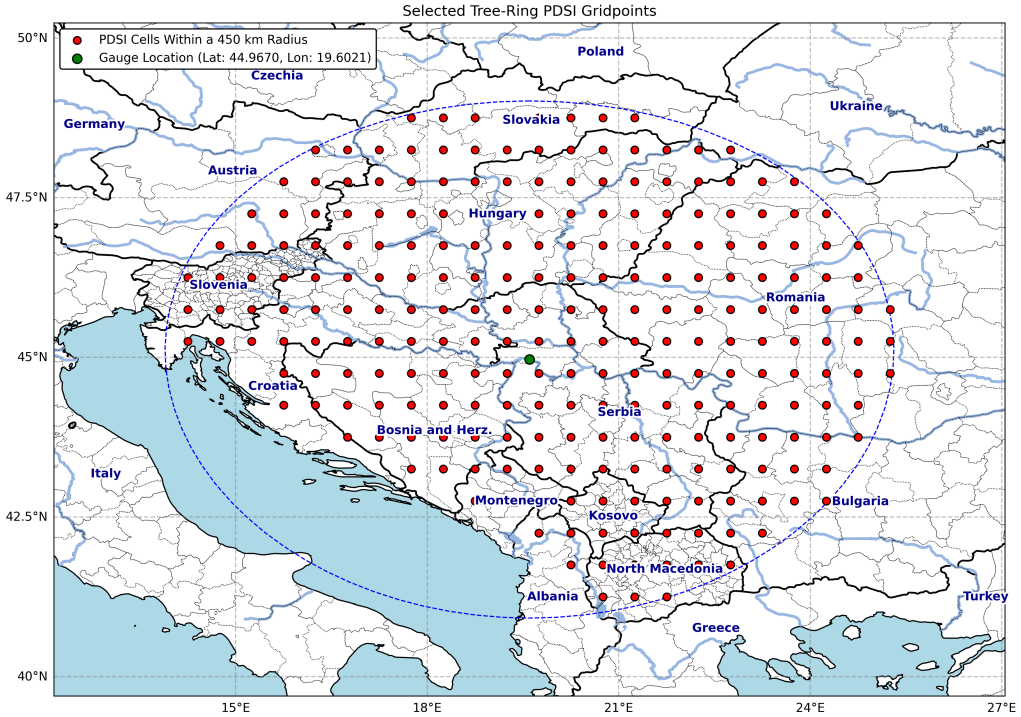

Figure 2. Self-calibrated Palmer Drought Severity Index (scPDSI) grid cells in a 450 km radius around the Sremska Mitrovica gauging station. Red dots indicate the selected scPDSI grid cells used in the analysis, while the green dot marks the location of the gauging station.

3.2. Machine Learning and Deep Learning Models

3.2.1. Machine Learning Models

We implemented nine Machine Learning (ML) models to reconstruct streamflow for the AMJJAS season, using the selected scPDSI cells as predictors and the observed

streamflow as the target variable. The methods were adapted based on the implementation described in [12]. The models included the following:

- **Linear Regression (LR)**: A baseline model employing the M5 Prime feature selection method to address collinearity and optimize variable selection.
- **Support Vector Machine (SVM)**: Configured with a linear kernel and scaled features for robust regression performance.
- **Deep Learning (DL)**: A basic two-layer neural network architecture with 50 neurons per layer and Rectified Linear Unit (ReLU) activation, optimized over 10 epochs.
- **Generalized Linear Model (GLM)**: Implemented with automatic family and link function selection, incorporating L2 regularization for robustness.
- **k-Nearest Neighbor (kNN)**: Configured with k = 5 and weighted voting, utilizing a mixed Euclidean distance measure.
- **Decisions Trees (DT)**: Tuned to balance simplicity and prediction accuracy, with a maximum depth of 10 and prepruning enabled.
- **Gradient Boosted Tree (GBT)**: Implemented with 50 trees, a maximum depth of 5, and a learning rate of 0.01.
- **Random Forest (RF)**: Configured with 100 trees, a maximum depth of 10, and confidence-based voting.
- **Gaussian Process (GP)**: Utilized a radial basis function (RBF) kernel to model non-linear relationships.

Each model was evaluated using 10-fold cross-validation to ensure robust performance metrics, including Root Mean Squared Error (RMSE) and the coefficient of determination (R^2).

3.2.2. Deep Learning Models

Two DL architectures were developed and tested:

- **Three-layer neural network**: Comprising hidden layers with 500, 100, and 50 neurons, respectively, using ReLU activation. This architecture was implemented following the approach outlined in [12], which demonstrated its effectiveness in capturing key features for similar tasks. Training was conducted over 40 epochs with the Adam optimizer (learning rate = 0.005), incorporating early stopping to prevent overfitting. Data were split into 70% training and 30% validation, and alternatively into 80% training and 20% validation to assess sensitivity to data partitioning.
- **Six-layer neural network**: Designed with decreasing neuron counts (248, 124, 62, 31, 15, and 7 neurons per layer) to not only reduce dimensionality gradually but also to explore the effects of increasing depth while reducing model complexity. This architecture was inspired by the work in [12], extending the approach to test whether a deeper structure could yield improved predictive performance. The model leveraged similar activation and optimization settings to the three-layer model and was evaluated using both 70:30 and 80:20 data splits.

For both DL architectures, the models were iteratively trained over 2000 configurations using a loop-based optimization framework to identify the best-performing configuration based on RMSE and R^2 metrics.

Both DL architectures, along with the ML models described earlier, underwent a post-prediction bias correction process using the RQUANT method [29]. RQUANT, a quantile-mapping approach, adjusts systematic discrepancies between predicted and observed values, thereby enhancing the reliability and interpretability of the reconstructions. This method was applied uniformly across all models to ensure comparability and to mitigate systematic errors that could arise from the inherent limitations of the training data.

4. Results

Streamflow Reconstruction

The observed daily streamflow values in m^3/s were aggregated to monthly volumes in Million-Cubic-Meters (MCM) and the April–May–June–July–August–September (AMJJAS) season was selected. Subsequently, the Machine Learning (ML) and Deep Learning (DL) models described in Section 3.2 were evaluated using validation datasets unseen by the models. Performance metrics, including Root Mean Squared Error (RMSE) and the coefficient of determination (R^2), are summarized in Table 1. These results highlight the varying degrees of accuracy and predictive power of each model.

Table 1. Performance metrics of tested ML and DL models over validation datasets.

Machine Learning Models	**RMSE**	**R^2**
Linear Regression (LR)	12,433.3	0.140
Support Vector Machine (SVM)	5714.5	0.430
Deep Learning (DL)	5738.0	0.226
Generalized Linear Model (GLM)	5239.4	**0.453**
k-Nearest Neighbor (kNN)	5295.1	0.264
Decisions Trees (DT)	6193.3	0.229
Gradient Boosted Tree (GBT)	**5121.1**	0.331
Random Forest (RF)	**4562.3**	**0.432**
Gaussian Process (GP)	22,382.4	0.035
Deep Learning Models	**RMSE**	**R^2**
3-Layer (70:30)	3421.0	0.629
3-Layer (80:20)	3091.4	0.546
6-Layer (70:30)	3369.4	0.622
6-Layer (80:20)	**2633.7**	**0.733**

Among the ML models, GLM, GBT, and RF achieved the best performance metrics. In contrast, the six-Layer (80:20) DL model stood out as the most accurate overall, significantly outperforming all ML models. To better understand the behavior of these models, their predictions were analyzed against observed data, and bias corrections were applied using the RQUANT method, which has been shown to effectively adjust for systematic errors in paleoclimatic reconstructions [29]. Figure 3 illustrates the comparison between observed streamflow, predicted values, and bias-corrected predictions for GLM, GBT, RF, and the six-layer (80:20) model. While GLM (Figure 3a) and GBT (Figure 3b) predictions capture the general trends of the observed data, they exhibit notable discrepancies in magnitude prior to bias correction. In contrast, the predictions of RF (Figure 3c) and the six-layer (80:20) DL model (Figure 3d) align more closely with the observed data, requiring only minor adjustments through bias correction. After applying bias correction, the predictions of GLM and GBT show magnitudes comparable to the observed data, indicating that bias correction effectively bridges the gap for these models, while adjustments to the predictions of RF and DL are comparatively smaller, further affirming their intrinsic accuracy.

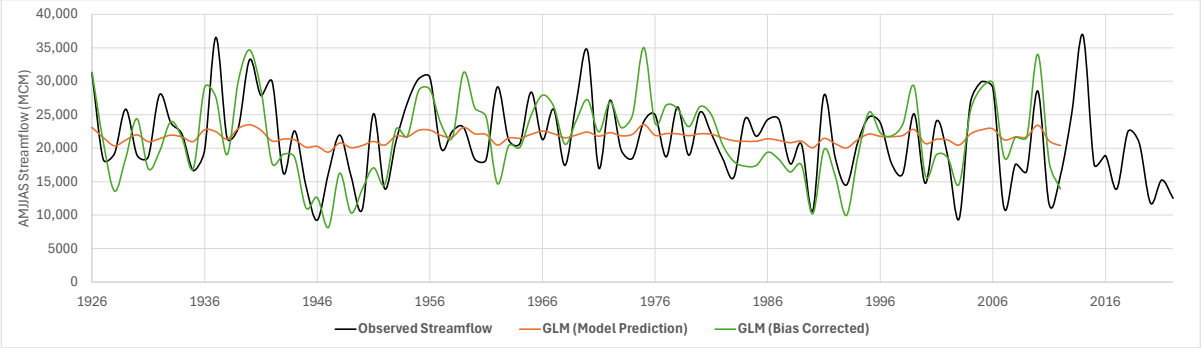

(**a**) Generalized Linear Model (GLM)

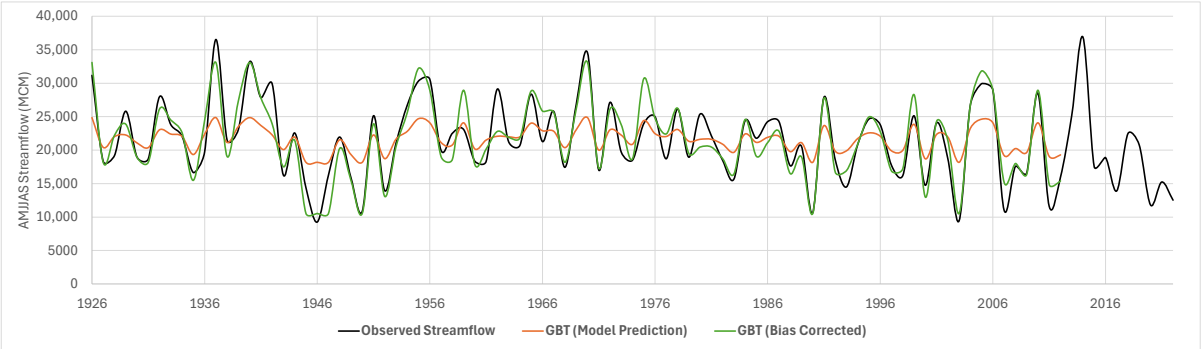

(**b**) Gradient Boosted Tree (GBT)

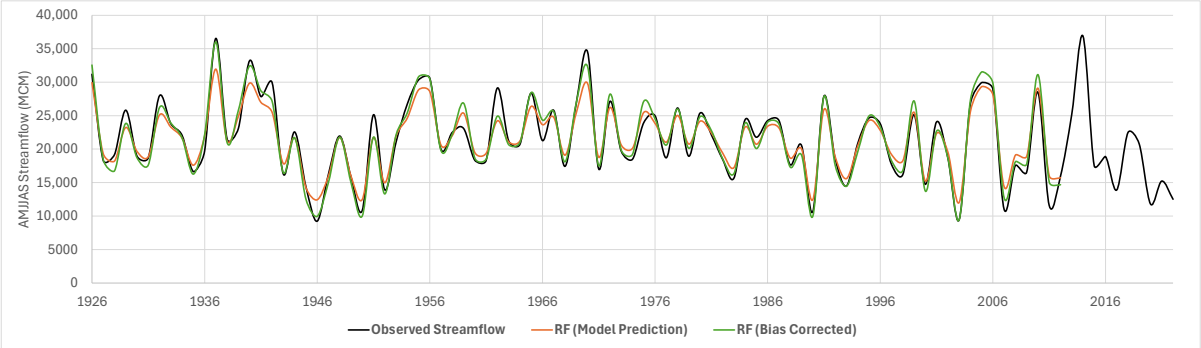

(**c**) Random Forest (RF)

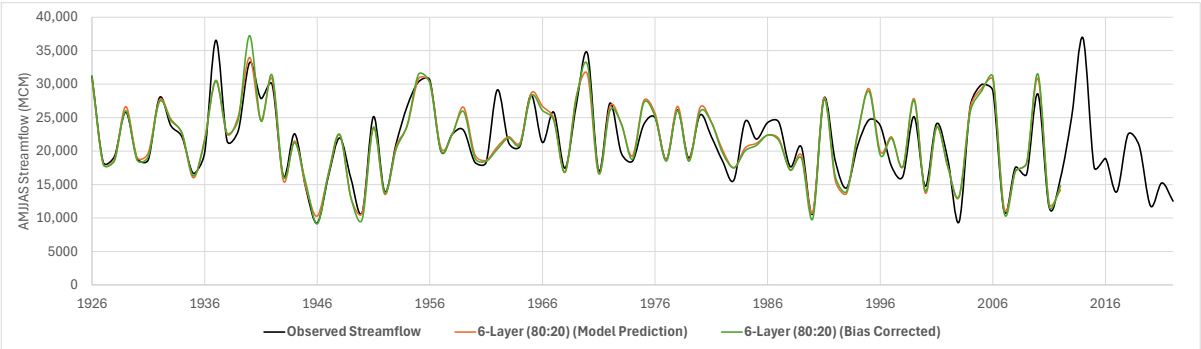

(**d**) 6-Layer Deep Learning Model (80:20)

Figure 3. Comparative analysis of streamflow predictions using (**a**) GLM, (**b**) GBT, (**c**) RF, and (**d**) 6-layer DL model (80% training/20% validation). Orange line: predicted streamflow; green line: bias-corrected streamflow prediction; blue line: observed streamflow.

Residual analysis was conducted to evaluate the homoscedasticity of these models, with the results displayed in Figure 4. This analysis revealed that GLM (Figure 4a) and GBT (Figure 4b) exhibited marked heteroscedastic behavior, showing reduced sensitivity to extreme values. However, bias correction mitigated this behavior to some extent, suggesting a higher degree of uncertainty in their predictions. Although the RF model (Figure 4c) also showed larger errors for extreme values (particularly for high-streamflow values, where predictions tended to be lower than observations), it displayed relatively more homoscedastic behavior compared to GBT and GLM. Lastly, the six-layer (80:20) DL model (Figure 4d) demonstrated the most homoscedastic behavior among all evaluated models, excelling in handling both extreme values and regular streamflow with high accuracy, demonstrating consistent performance across all ranges of observed data.

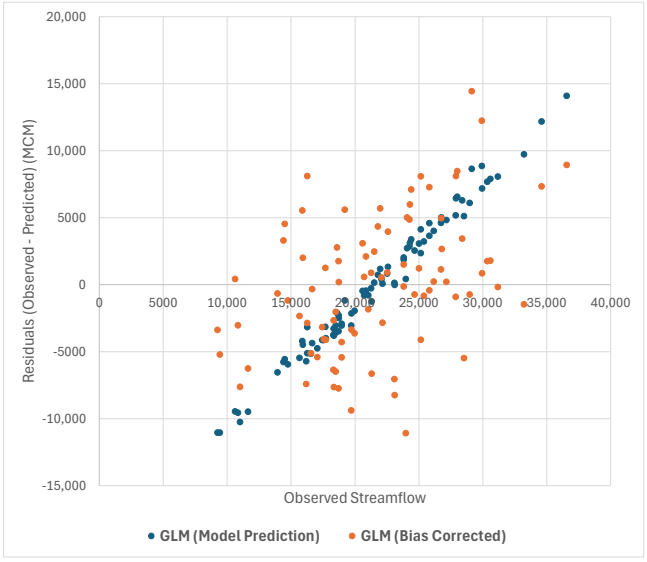

(**a**) Generalized Linear Model (GLM)

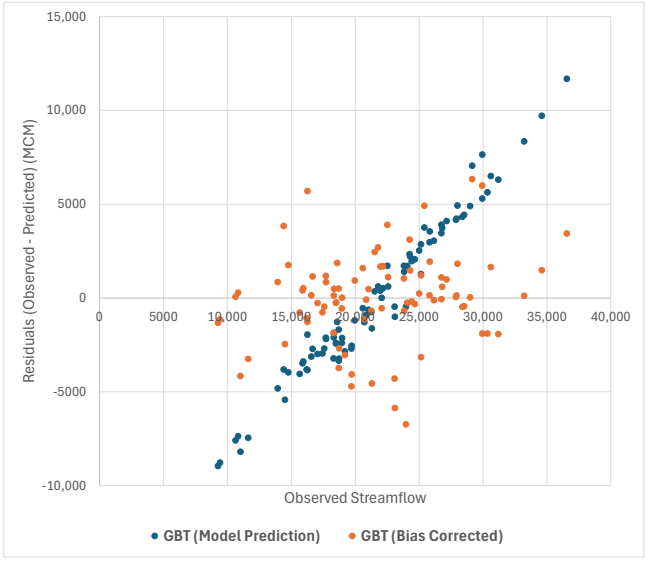

(**b**) Gradient Boosted Tree (GBT)

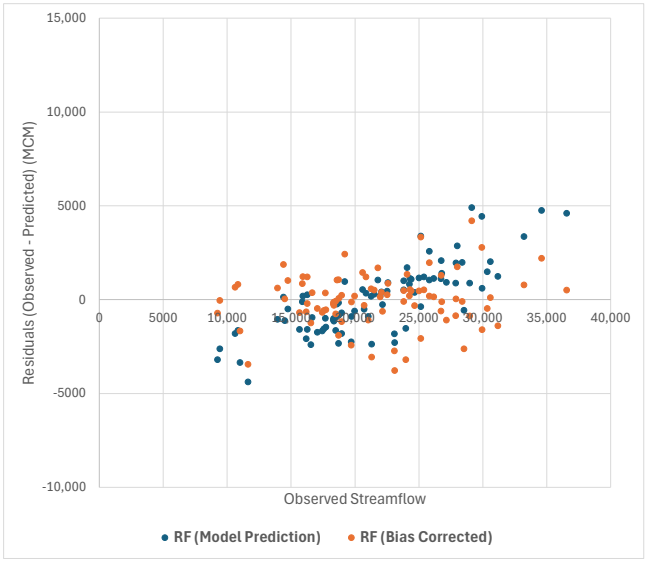

(**c**) Random Forest (RF)

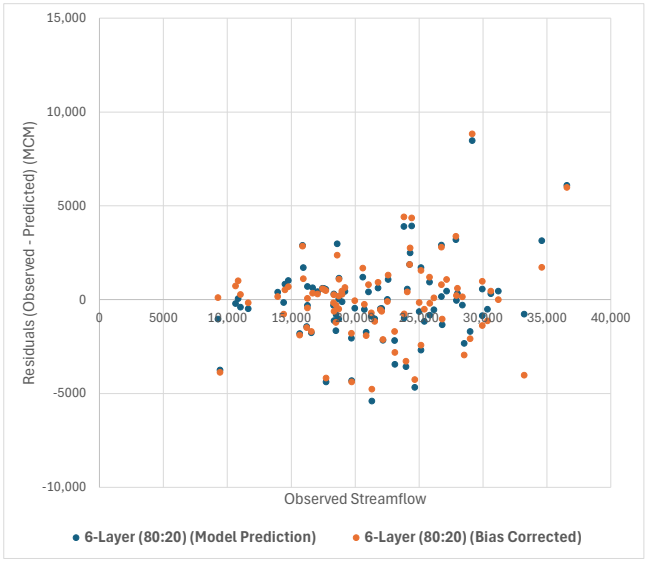

(**d**) Six-layer Deep Learning model (80:20)

Figure 4. Residual analysis using (**a**) GLM, (**b**) GBT, (**c**) RF, and (**d**) the six-layer DL model (80% training/20% validation). Blue dots: observed streamflow–oredicted streamflow; orange dots: observed streamflow–bias-corrected predicted streamflow.

The superior performance of the six-layer DL model can be attributed to its ability to capture complex, non-linear relationships between self-calibrated Palmer Drought Severity Index (scPDSI) proxies and streamflow dynamics. The progressive reduction in neuron counts across layers facilitated dimensionality reduction while preserving key features, enabling the model to generalize effectively. This deeper architecture demonstrated a higher capacity to identify intricate patterns, as evidenced by the consistent alignment of its predictions with observed data and its reduced sensitivity to errors across the range of streamflow values, even prior to bias correction.

The historic (1926 to 2022) record revealed that 2000 to 2022 was the lowest 23-year period, resulting in an average annual AMJJAS streamflow of 19,524 MCM. The use of scPDSI as a tree-ring-based reconstruction proxy allowed for the development of streamflow reconstruction models back to 0 CE (~2000 years). A 23-year end-year filter was applied to the four reconstruction models: GLM BC, GBT BC, RF BC, and six-layer DL model (80% training/20% validation) BC (Figure 5a). A visual inspection of the individual plots of each model (Figure 5a) shows favorable, temporal agreement and each model shows a similar scale in pluvial (wet) and drought (dry) periods. The average of the four models was next evaluated with uncertainty (5th and 95th percentiles—gray) (Figure 5b). The 2000 to 2022 23-year historic low flow (average of 19,524 MCM) is provided (red line).

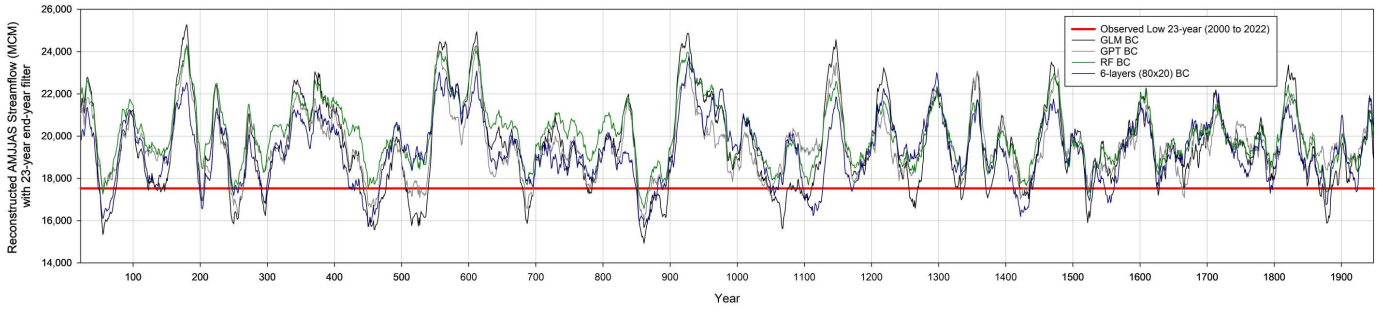

(**a**) Individual reconstructions

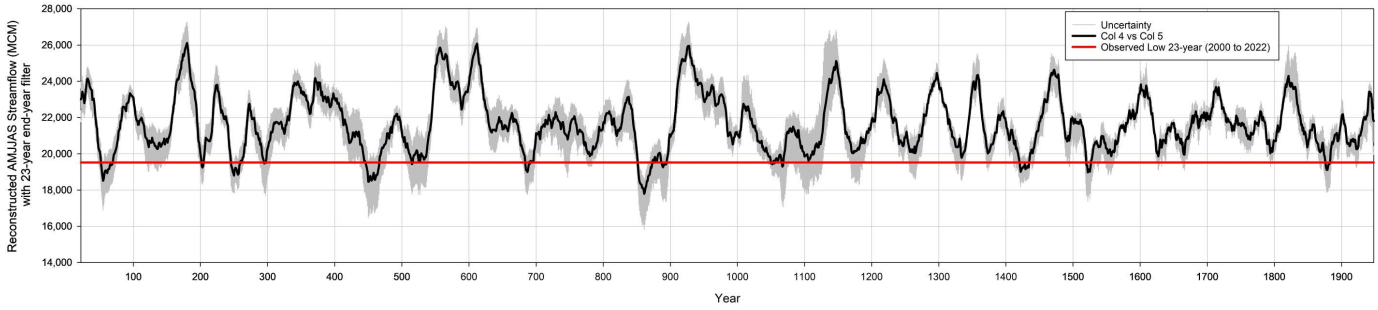

(**b**) Average reconstructions

Figure 5. Reconstructed AMJJAS streamflow (MCM) with 23-year end-year filter: (**a**) Individual GLM BC, GBT BC, RF BC, and 6-layer Deep Learning model (80% training/20% validation) BC models with 2000 to 2022 low flow (red line). (**b**) Average of GLM BC, GBT BC, RF BC, and 6-layer Deep Learning model (80% training/20% validation) BC models with uncertainty (5th and 95th percentile, gray area) with 2000 to 2022 low flow (red line).

5. Discussion

The development of Machine Learning (ML) models for streamflow reconstruction represents a relatively recent shift in the field, diverging from traditional statistical approaches like Stepwise Linear Regression (SLR). While ML models are powerful in their ability to identify complex relationships in data, their performance is inherently tied to the volume and quality of the training data. In this study, the limited availability of training data

(97 years) posed challenges for these models to fully capture the variability and dynamics of streamflow. However, the bias correction applied to the predictions was essential in mitigating these limitations.

Figures 3–5 illustrate the impact of bias correction on the predictions of the Generalized Linear Model (GLM) and Gradient Boosted Tree (GBT). Before bias correction, these models, while able to capture the general trends in the observed data, exhibited significant deviations in magnitude, particularly for extreme values. Bias correction not only improved the consistency of their predictions with the observed data but also aligned their reconstructed streamflow behavior with the Random Forest (RF) and 6-Layer (80:20) Deep Learning (DL) models, which showed better agreement with the observed data initially. This adjustment demonstrates the role of bias correction in reducing systematic errors and improving the reliability of predictions, even when working with models trained on limited datasets.

The residual analysis further supports this observation. Prior to bias correction, the GLM and GBT models displayed heteroscedasticity, with errors varying substantially across the range of observed values. Bias correction reduced this heteroscedasticity, suggesting a more consistent model performance across different flow regimes. While the corrected predictions still indicate a higher degree of uncertainty for these models, they also suggest that the general trends captured by GLM and GBT are valid and robust. This highlights the utility of bias correction in refining the predictive capacity of ML models in contexts where training data are constrained.

Another important finding from this study relates to the reconstruction of long-term drought periods, offering insights into the historical context of recent low-flow conditions. When evaluating past 23-year drought intervals (Figure 5b), the 2000–2022 period ranked as the 14th lowest flow period in the past ~2000 years and the third lowest over the last ~600 years. Notable paleo-drought intervals include 861 CE (17,792 Million-Cubic-Meters (MCM)), 450 CE (18,453 MCM), 55 CE (18,515 MCM), 250 CE (18,800 MCM), 1522 CE (18,977 MCM), 687 CE (18,995 MCM), 1422 CE (19,006 MCM), 1878 CE (19,112 MCM), 203 CE (19,241 MCM), 889 CE (19,257 MCM), 1067 CE (19,293 MCM), 515 CE (19,430 MCM), and 297 CE (19,491 MCM). These findings illustrate the historical severity and frequency of low-flow events, providing important reference points for understanding hydrological extremes over millennia. Furthermore, they are consistent with prior studies that reveal significant hydrological variability in the region, indicating that the integration of machine learning and deep learning approaches, together with bias correction, can enhance our understanding of historical hydrological extremes.

The historical variability in drought periods in the Sava River Basin highlights the urgent need for adaptive and integrated water management strategies to address ongoing and future climate challenges. The Sava riparian countries have experienced significant climatic changes, including rising temperatures, altered precipitation patterns, and increased extreme weather events such as prolonged droughts and localized intense rainfall, contributing to higher flood risks [30]. These changes pose substantial challenges to water resources, water quality, and key economic sectors such as agriculture, forestry, hydropower production, navigation, industry, tourism, and ecosystems [30]. Several regional water management strategies have been implemented to enhance climate resilience in the Sava River Basin (SRB). For example, the Sava River Basin Management Plan focuses on reducing water pollution and addressing hydromorphological alterations through coordinated measures across the basin [31]. Similarly, the Framework Agreement on the SRB promotes transboundary cooperation among Bosnia and Herzegovina, Croatia, Slovenia, and Serbia to support sustainable water use. Additionally, the Water and Climate Adaptation Plan (WATCAP) integrates climate resilience into policy planning through hydrological

modeling and climate assessments [32]. Future projections indicate increasing droughts and rising temperatures in the region, emphasizing the need for comprehensive and collaborative adaptation strategies [33].

These findings are not only relevant for understanding historical hydrological extremes but also have practical implications for water resource management. By providing detailed reconstructions of streamflow variability over millennia, this study offers valuable insights that can inform the development of more resilient strategies for managing water resources in the SRB and other regions facing similar challenges. The methodologies employed here can be adapted to improve the predictive capacity of hydrological models and support decision-making processes under changing climatic conditions.

Although this study demonstrates the effectiveness of ML and DL models in streamflow reconstruction, certain limitations should be acknowledged. The reliance on the self-calibrated Palmer Drought Severity Index (scPDSI) as a proxy introduces potential biases due to its assumptions, which may not fully align with the specific hydrological conditions of the SRB. Additionally, while bias correction proved useful in addressing challenges related to training data constraints, it also emphasizes the need to refine these methods. Future research could explore the integration of diverse proxies or advanced approaches, such as transfer learning, to enhance the robustness and adaptability of ML and DL models for paleohydrological applications.

Finally, while bias correction effectively adjusted the output of ML and DL models, it is essential to apply this technique judiciously to avoid introducing artifacts or misrepresentations in the reconstructions. As noted in [29], bias correction is not a substitute for accurate modeling but a complementary tool that, when used appropriately, can improve the reliability of reconstructions. Future studies should explore the integration of bias correction with model training processes, as well as the potential for hybrid models combining statistical and ML approaches, to leverage the strengths of both methodologies.

6. Conclusions

This study analyzed streamflow reconstruction in the Sava River Basin (SRB), applying Machine Learning (ML) and Deep Learning (DL) methods to investigate hydrological variability over extended temporal scales. The findings demonstrate how modern modeling techniques can effectively address the complexities of streamflow dynamics, particularly under constraints posed by limited observational records.

Among the models tested, ensemble methods such as Random Forest (RF) and Gradient Boosted Tree (GBT) showed a strong capacity for capturing streamflow patterns, while the six-layer DL model provided consistent accuracy in both predictive and reconstructive tasks. The use of bias correction across all models played a decisive role in reducing discrepancies between predicted and observed streamflow, particularly for models initially prone to greater variability in magnitude. This alignment ensured that reconstructed patterns remained consistent with historical hydrological conditions, providing meaningful insights into the drivers of streamflow variability.

The results highlight the severe hydrological conditions of the 21st century, with the Sava River (SR) experiencing one of its lowest 23-year flow intervals in the past ~500 years. Only the late 19th century displayed a comparable dry period. While the 23-year window was chosen to coincide with the end of this significant low-flow phase in 2022, similar trends of extended dryness may emerge under different temporal filters. The findings present 2022 as the endpoint of a pronounced multidecadal dry period in the basin.

Future research could enhance these approaches by combining ML and DL methods with traditional statistical techniques, potentially through hybrid models that integrate the predictive capabilities of advanced algorithms with the interpretability of statistical meth-

ods. Additionally, incorporating bias correction directly into the modeling process, rather than as a post-prediction adjustment, may further improve the accuracy and reliability of hydrological reconstructions. These methodological advancements could provide a more nuanced understanding of historical streamflow variability, supporting evidence-based decision-making for water resource management in an era of increasing climate variability.

Author Contributions: Conceptualization, A.A.R.M., I.L. and G.T.; methodology, A.A.R.M., I.L. and G.T.; software, A.A.R.M.; validation, A.A.R.M. and G.T.; formal analysis, A.A.R.M., I.L. and G.T.; investigation, A.A.R.M., I.L. and G.T.; resources, I.L.; data curation, A.A.R.M., I.L. and G.T.; writing—original draft preparation, A.A.R.M., I.L., G.T. and M.J.; writing—review and editing, A.A.R.M., I.L., G.T., J.G. and M.J.; visualization, A.A.R.M., G.T. and M.J.; supervision, G.T. and J.G.; project administration, A.A.R.M., I.L. and G.T.; funding acquisition, G.T. All authors have read and agreed to the published version of the manuscript.

Funding: This research was supported by the project 09I03-03-V04-00186 "Streamflow Drought Through Time", funded by the European Union's Next Generation EU as part of the Recovery and Resilience Plan of the Slovak Republic, specifically through the initiative for more efficient management and enhancement of funding for research, development, and innovation.

Data Availability Statement: The data supporting the results of this study are available and archived at https://alabama.box.com/s/log4ri5lu0jw61e5m9ze8r8slf0nv8yc, accessed on 24 December 2024.

Acknowledgments: The authors wish to thank The University of Alabama, Alabama Water Institute (AWI), and the Cooperative Institute for Research to Operations in Hydrology (CIROH) for their support. This project is supported by the National Science Foundation Research Traineeship (NSF NRT), Water: Research to Operations (Water: R2O) (2152140) at The University of Alabama, and by the National Oceanic and Atmospheric Administration (NOAA), awarded to CIROH through the NOAA Cooperative Agreement with The University of Alabama, NA22NWS4320003.

Conflicts of Interest: The authors declare no conflicts of interest.

Abbreviations

The following abbreviations are used in this manuscript:

AMJJAS	April–May–June–July–August–September
DL	Deep Learning
DR	Danube River
DT	Decisions Trees
GBT	Gradient Boosted Tree
GLM	Generalized Linear Model
GP	Gaussian Process
kNN	k-Nearest Neighbor
LR	Linear Regression
MCM	Million-Cubic-Meters
ML	Machine Learning
OWDA	Old World Drought Atlas
R^2	coefficient of determination
RBF	radial basis function
ReLU	Rectified Linear Unit
RF	Random Forest
RHSS	Republic Hydrometeorological Service of Serbia
RMSE	Root Mean Squared Error
scPDSI	self-calibrated Palmer Drought Severity Index
SLR	Stepwise Linear Regression
SR	Sava River
SRB	Sava River Basin

SVM	Support Vector Machine
WATCAP	Water and Climate Adaptation Plan
WMO	World Meteorological Organization

References

1. Gholami, V.; Sahour, H.; Torkaman, J. Reconstruction of springs discharge using tree-rings and earlywood vessel chronologies in an alluvial aquifer. *Ecol. Inform.* **2021**, *64*, 101363. [CrossRef]
2. Okello, C.; Tomasello, B.; Greggio, N.; Wambiji, N.; Antonellini, M. Impact of Population Growth and Climate Change on the Freshwater Resources of Lamu Island, Kenya. *Water* **2015**, *7*, 1264–1290. [CrossRef]
3. Wise, E.K. Tree ring record of streamflow and drought in the upper Snake River. *Water Resour. Res.* **2010**, *46*, W11529. [CrossRef]
4. Ballesteros-Cánovas, J.A.; Stoffel, M.; Benito, G.; Rohrer, M.; Barriopedro, D.; García-Herrera, R.; Beniston, M.; Brönnimann, S. On the extraordinary winter flood episode over the North Atlantic Basin in 1936. *Ann. N. Y. Acad. Sci.* **2019**, *1436*, 206–216. [CrossRef]
5. Wilhelm, B.; Ballesteros Cánovas, J.A.; Macdonald, N.; Toonen, W.H.; Baker, V.; Barriendos, M.; Benito, G.; Brauer, A.; Corella, J.P.; Denniston, R.; et al. Interpreting historical, botanical, and geological evidence to aid preparations for future floods. *WIREs Water* **2019**, *6*, e1318. [CrossRef]
6. Anderson, S.; Ogle, R.; Tootle, G.; Oubeidillah, A. Tree-Ring Reconstructions of Streamflow for the Tennessee Valley. *Hydrology* **2019**, *6*, 34. [CrossRef]
7. Meko, M.D.; Therrell, M.D. A record of flooding on the White River, Arkansas derived from tree-ring anatomical variability and vessel width. *Phys. Geogr.* **2020**, *41*, 83–98. [CrossRef]
8. Zhang, T.; Liu, Y.; Zhang, R.; Yu, S.; Fan, Y.; Shang, H.; Jiang, S.; Qin, L.; Zhang, H. Tree-ring width based streamflow reconstruction for the Kaidu River originating from the central Tianshan Mountains since A.D. 1700. *Dendrochronologia* **2020**, *61*, 125700. [CrossRef]
9. Kern, Z.; Németh, A.; Horoszné Gulyás, M.; Popa, I.; Levanič, T.; Hatvani, I.G. Natural proxy records of temperature- and hydroclimate variability with annual resolution from the Northern Balkan–Carpathian region for the past millennium—Review & recalibration. *Quat. Int.* **2016**, *415*, 109–125. [CrossRef]
10. Ljungqvist, F.C.; Seim, A.; Krusic, P.J.; González-Rouco, J.F.; Werner, J.P.; Cook, E.R.; Zorita, E.; Luterbacher, J.; Xoplaki, E.; Destouni, G.; et al. European warm-season temperature and hydroclimate since 850 CE. *Environ. Res. Lett.* **2019**, *14*, 084015. [CrossRef]
11. Tootle, G.; Oubeidillah, A.; Elliott, E.; Formetta, G.; Bezak, N. Streamflow Reconstructions Using Tree-Ring-Based Paleo Proxies for the Sava River Basin (Slovenia). *Hydrology* **2023**, *10*, 138. [CrossRef]
12. Ramírez Molina, A.A.; Bezak, N.; Tootle, G.; Wang, C.; Gong, J. Machine-Learning-Based Precipitation Reconstructions: A Study on Slovenia's Sava River Basin. *Hydrology* **2023**, *10*, 207. [CrossRef]
13. Viorica, N.; Cătălin-Constantin, R.; Andrei, M.; Știrbu Marian-Ionuț.; Ionel, P.; Monica, I. The first tree-ring reconstrruction of streamflow variability over the last ~250 years in the Lower Danube. *J. Hydrol.* **2023**, *617*, 129150. [CrossRef]
14. Cook, E.R.; Seager, R.; Kushnir, Y.; Briffa, K.R.; Büntgen, U.; Frank, D.; Krusic, P.J.; Tegel, W.; van der Schrier, G.; Andreu-Hayles, L.; et al. Old World megadroughts and pluvials during the Common Era. *Sci. Adv.* **2015**, *1*, e1500561. [CrossRef]
15. Trlin, D.; Mikac, S.; Žmegač, A.; Orešković, M. Dendrohydrological Reconstructions Based on Tree-Ring Width (TRW) Chronologies of Narrow-Leaved Ash in the Sava River Basin (Croatia). *Sustainability* **2021**, *13*, 2408. [CrossRef]
16. Dolinaj, D.; Leščešen, I.; Pantelić, M.; Urošev, M.; Milijašević-Joksimović, D. Danube River discharge at Bezdan gauging station (Serbia) and its correlation with atmospheric circulation patterns. *Geogr. Pannonica* **2019**, *23*, 14–22. [CrossRef]
17. Gnjato, S.; Leščešen, I.; Basarin, B.; Popov, T. What is happening with frequency and occurrence of the maximum river discharges in Bosnia and Herzegovina? *Acta Geogr. Slov.* **2024**, *64*, 129–149. [CrossRef]
18. Leščešen, I.; Šraj, M.; Pantelić, M.; Dolinaj, D. Assessing the impact of climate on annual and seasonal discharges at the Sremska Mitrovica station on the Sava River, Serbia. *Water Supply* **2021**, *22*, 195–207. [CrossRef]
19. Ho, M.; Lall, U.; Sun, X.; Cook, E.R. Multiscale temporal variability and regional patterns in 555 years of conterminous U.S. streamflow. *Water Resour. Res.* **2017**, *53*, 3047–3066. [CrossRef]
20. Formetta, G.; Tootle, G.; Bertoldi, G. Streamflow Reconstructions Using Tree-Ring Based Paleo Proxies for the Upper Adige River Basin (Italy). *Hydrology* **2022**, *9*, 163. [CrossRef]
21. Formetta, G.; Tootle, G.; Therrell, M. Regional Reconstruction of Po River Basin (Italy) Streamflow. *Hydrology* **2022**, *9*, 163. [CrossRef]
22. International Sava River Basin Commission (ISRBC). *2nd Sava River Basin Analysis Report*; Technical Report; Accepted by ISRBC at Its 46th Session on 15 June 2017; International Sava River Basin Commission (ISRBC): Zagreb, Croatia, 2016.
23. Dolšak, D.; Bezak, N.; Šraj, M. Temporal characteristics of rainfall events under three climate types in Slovenia. *J. Hydrol.* **2016**, *541*, 1395–1405. [CrossRef]

24. Lavtar, K.; Bezak, N.; Šraj, M. Rainfall-Runoff Modeling of the Nested Non-Homogeneous Sava River Sub-Catchments in Slovenia. *Water* **2020**, *12*, 128. [CrossRef]
25. Šraj, M.; Bezak, N. Comparison of time trend- and precipitation-informed models for assessing design discharges in variable climate. *J. Hydrol.* **2020**, *589*, 125374. [CrossRef]
26. Leščešen, I.; Gnjato, S.; Galinović, I.; Basarin, B. Hydrological drought assessment of the Sava River basin in South-Eastern Europe. *J. Water Clim. Chang.* **2024**, *15*, 3902–3918. [CrossRef]
27. Leščešen, I.; Basarin, B.; Podraščanin, Z.; Mesaroš, M. Changes in Annual and Seasonal Extreme Precipitation over Southeastern Europe. *Environ. Sci. Proc.* **2023**, *26*, 48. [CrossRef]
28. Orešić, D.; Čanjevac, I.; Plantak, M. Changes in flow and the discharge regime on the Ilova river. *Acta Geogr. Croat.* **2017**, *43/44*, 1, 1–20. Available online: https://hrcak.srce.hr/216383 (accessed on 24 December 2024).
29. Robeson, S.M.; Maxwell, J.T.; Ficklin, D.L. Bias Correction of Paleoclimatic Reconstructions: A New Look at 1,200+ Years of Upper Colorado River Flow. *Geophys. Res. Lett.* **2020**, *47*, e2019GL086689. [CrossRef]
30. International Sava River Basin Commission. *2nd Sava River Basin Management Plan*; International Sava River Basin Commission: Zagreb, Croatia, 2022. Digital Version. Available online: https://www.savacommission.org/en/2nd-sava-river-basin-management-plan/10461 (accessed on 4 November 2024).
31. Grošelj, S. Integration of Measures in the Sava River Basin Management Plan. In Proceedings of the 1st Danube Region Workshop, 2014, Szentendre, Hungary, 28–29 January 2014. Digital Version. Available online: https://www.nwrm.eu/sites/default/files/regional-workshops/Danube/sessionIII/S-3-2.Integration_into_Sava_Management_SGroselj.pdf (accessed on 4 November 2024).
32. World Bank Group. *Water and Climate Adaptation Plan for the Sava River Basin: Main Report*; World Bank Group: Washington, DC, USA, 2015. Digital Version. Available online: http://documents.worldbank.org/curated/en/847991468189271629/Main-report (accessed on 4 November 2024).
33. Meerbach, D.; Kindler, J.; Shanahan, P.; Strzepek, K. *Implications of Climate Change for Sava River Basin Water Management*; The World Bank: Sarajevo, Bosnia and Herzegovina, 18–20 May 2009. Digital Version. Available online: https://unece.org/fileadmin/DAM/env/water/meetings/Sarajevo_workshop/presentations/session2/Meerbach_Kindler.pdf (accessed on 4 November 2024).